Dynamics of 1,3-butadiene adsorbed in Na-Y zeolite: A molecular dynamics simulation study

Siddharth Gautam, S. Mitra, S. L. Chaplot, and R. Mukhopadhyay*
Solid State Physics Division, Bhabha Atomic Research Centre, Mumbai-400 085, India
(Received 11 April 2008; published 16 June 2008)

Here we report dynamics of 1,3-butadiene molecules adsorbed in Na-Y zeolite as studied using molecular dynamics (MD) simulations. The results showed that the translational motion of the guest molecule exists in three different time scales one of which matches well with the quasielastic neutron scattering (QENS) measurement reported earlier. The translational motion in the component, which has been measured by QENS, is found to occur through discrete jumps, in agreement with the analysis of the experiments. The diffusion coefficients obtained from the correlation functions are compared to those obtained earlier for other hydrocarbons in Na-Y zeolite from MD simulation studies. The diffusion of 1,3-butadiene is found to be slower than that of acetylene but faster than that of propane. The rotational motion is found to be isotropic in nature. Rotational diffusion coefficient of 1,3-butadiene is found to be smaller than that of propane in Na-Y as expected due to the larger inertia of the former.

DOI: 10.1103/PhysRevE.77.061201 PACS number(s): 51.20.+d, 02.70.−c, 51.90.+r

I. INTRODUCTION

Diffusion of hydrocarbons in zeolites has attracted a great deal of attention in research because of both fundamental and applied interests. The well ordered porous structure of zeolites makes them an ideal model to experimentally study the phenomenon of molecular dynamics in confined geometries. Because of their pores with typical sizes of the order of a few angstrom, zeolites have found a variety of applications as molecular sieves. Several properties of zeolites, such as selective adsorption of host molecules and acid strength, make them very good catalysts. They are therefore used in the petrochemical industry [1,2]. The catalytic property of the zeolites depends upon, in addition to several other factors, the approach of the adsorbed molecules toward the reaction sites and also the ease with which the reactants and the products can be separated because of the difference in their diffusivities. This implies that in order to understand the catalytic properties of zeolites it is imperative to study the diffusion of molecules adsorbed in zeolitic cages. This depends upon many factors that include the host-zeolite interaction, the shape of the host, the volume of the cages, and their potential energy landscape, temperature, etc. All of this makes the study of diffusion of hydrocarbons in zeolites indispensable.

Studies of diffusive dynamics have been reported using a variety of formalisms and techniques including quasielastic neutron scattering [3–10], molecular dynamics (MD) simulations [6,7,10–14], percolation theory [15], nuclear magnetic resonance (NMR) [16], and recently neutron spin-echo (NSE) [17,18]. A widely used zeolite is the Na-Y zeolite, which has especially large cavities called supercages. These supercages have a diameter of 11.8 Å and are interconnected by 12-member oxygen rings with a diameter of 7 Å. Quasielastic neutron scattering (QENS) studies on diffusion of propane [6,7], acetylene [8,10], and 1,3-butadiene [9] in Na-Y zeolite cages have been reported. The studies on propane and acetylene were supplemented by MD simulation studies [6,7,10,12]. A comparison of diffusivities of these three molecules in the zeolitic cages has also been attempted [9]. It was suggested that the dynamics observed in the QENS experiments on 1,3-butadiene in Na-Y zeolite might be just a part of a more complex dynamics as was found to be the case in earlier studies on propane and acetylene. This could be resolved by the MD simulation studies of 1,3-butadiene in Na-Y zeolite. In addition to this, more insights are expected to be gained from a simulation study. We report here the MD simulation studies of 1,3-butadiene in Na-Y zeolite.

II. COMPUTATIONAL DETAILS

Na-Y zeolite atomic positions as reported by Fitch *et al.* [19] were used in the simulation. One unit cell of Na-Y zeolite in a cubic simulation cell of length 24.8536 Å was used. Butadiene molecules were loaded with a concentration of four molecules per zeolite cage, which is also the saturation value, and attempts for any further loading were futile. A simulation time step of 1.0 fs was used. This yielded good energy conservation. The temperature was scaled to 300 K at every calculation step up to the first 300 ps followed by an equilibration for 100 ps during which no storing of the configurations was done. This was followed by a run for 1.3 ns during which configurations were stored at intervals of 0.02 ps and averages for various quantities were calculated from them. 1,3-butadiene molecules were considered to be rigid and were modeled in the united atom model where one 1,3-butadiene molecule is considered to be made up of two CH_2 sites connected to two CH sites separated from each other by a distance of 1.451 Å. The CH_2-CH distance taken was 1.335 Å. The molecule was taken to be planar as shown in Fig. 1 with CH_2-CH-CH angles measuring 123.4° each. The zeolite framework atoms were kept fixed throughout the simulation. Ghorai *et al.* [11] have shown that the presence of extra-framework cations has only a marginal effect on the diffusivities of the adsorbed species although the adsorption

*Corresponding author; mukhop@barc.gov.in; FAX: +91-22-25505151

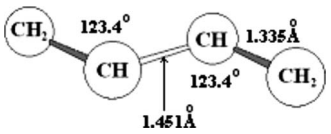

FIG. 1. A schematic of 1,3-butadiene molecule with united atom model as used in the simulation.

properties are affected to a considerable extent by their presence as shown by Calero *et al.* [20]. Therefore, the extra-framework cations were also kept immobile in the present simulation. All simulations were carried out using leapfrog form of Verlet algorithm in microcanonical ensemble [21]. Cubic periodic boundary conditions were used and all Lennard-Jones interactions were truncated at 12.0 Å. Rotational motion was accounted for by following the change in the orientations of the molecule specified by quaternion parameters.

The guest-guest as well as the guest-zeolite interactions were modeled by the (6-12) Lennard-Jones potential given by

$$\Phi(r_{ij}) = 4\varepsilon_{ij}\left[\left(\frac{\sigma_{ij}}{r_{ij}}\right)^{12} - \left(\frac{\sigma_{ij}}{r_{ij}}\right)^{6}\right], \tag{1}$$

where ε_{ij} is the well depth, σ_{ij} is the diameter, and r_{ij} is the distance between the interacting sites i and j. As the bulkier oxygen's surround the Si and Al atoms, the close approach of guest to Si and Al atoms is not possible. Therefore, interactions of the guest molecules with Si and Al are not considered. The potential parameters (Table I) were taken from the literature [11,22]. In the present work we have chosen to neglect the polarization interaction between the guest molecules and the zeolitic atom because this interaction contributing typically only a few percent of the total interaction energy, may not alter the self-diffusivity significantly [11], on the other hand, its inclusion can make the simulation rather costly.

In Fig. 2 we show the potential energy landscape as seen by a CH site due to the zeolite in the $z=10$ Å plane. The two landscapes show the potential energy due to the zeolitic atoms at different resolutions. Because of very high potential energies at some points the potential is plotted in logarithmic scale in Fig. 2(a). However, this conceals several interesting features that are to be seen at points with lower potential energy values. To overcome this limitation, the same landscape is replotted in Fig. 2(b) by making all positive energies equal to 0. As can be seen, from Fig. 2(a) there are several very-low-energy (shown hatched) regions. These are cross sections of the supercages. On resolving these regions further, a structure can be seen in Fig. 2(b) where within the same cage, several regularly arranged favorable positions could be found for a guest molecule where the potential energy is minimum (shown as darkened regions). Indeed as can be seen in Fig. 2 the sites of minimum energy in the potential energy landscape looks very well ordered. This ordering plays an important role in the mechanism of diffusion, as we shall see shortly.

TABLE I. Intermolecular potential parameters for molecule-molecule and molecule-zeolite interactions.

Interaction	σ_{ij}(Å)	ε_{ij}(K)
CH_2-CH_2	3.85	70.462
CH_2-CH	3.825	63.8616
CH-CH	3.8	57.8795
CH_2-O	3.2	104.2861
CH-O	3.175	94.5173
CH_2-Na	3.61	18.3889
CH-Na	3.585	16.6663

III. RESULTS AND DISCUSSION

Translation as well as rotational motion can be present in the case of molecular systems. For a molecular system the translational motion pertains to the motion of the center of mass and rotational motion is accounted for by following the motion of the constituent atoms about the center of mass. Often these motions appear as dynamically independent when their time scales are very different. As we shall see later, this assumption is fairly valid in the present case.

Correlation functions calculated from an MD simulation reveal a lot of information about the system under study.

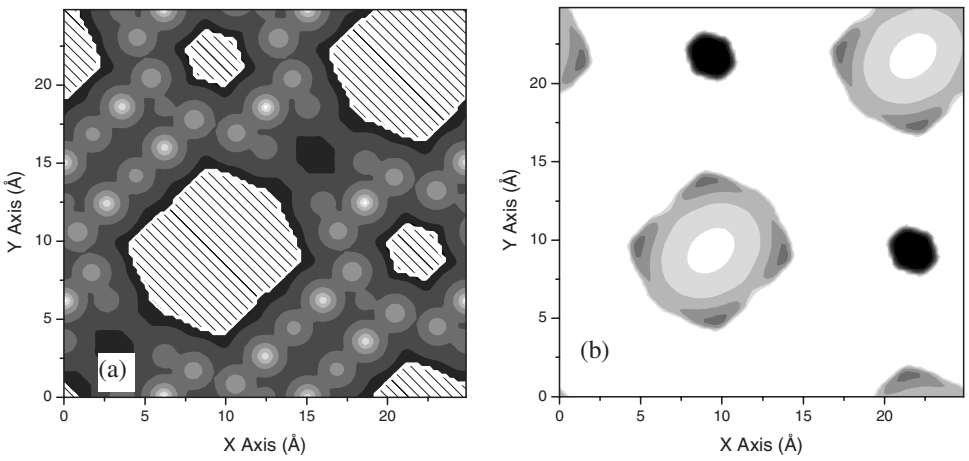

FIG. 2. (a) A cross section of the potential energy landscape of Na-Y zeolite as seen by a CH site. The hatched regions indicate the cages. (b) shows the potential energy within the cage where a darker region indicates highly negative potential. Four distinct regions of regularly arranged potential minima could easily be seen.

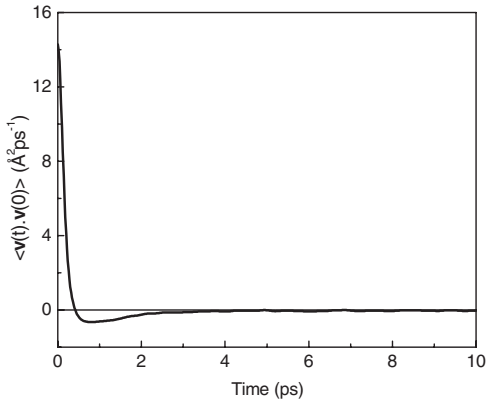

FIG. 3. Variation of center-of-mass velocity autocorrelation function with time. A negative region is indicative of the rebounding motion due to collisions of the molecules.

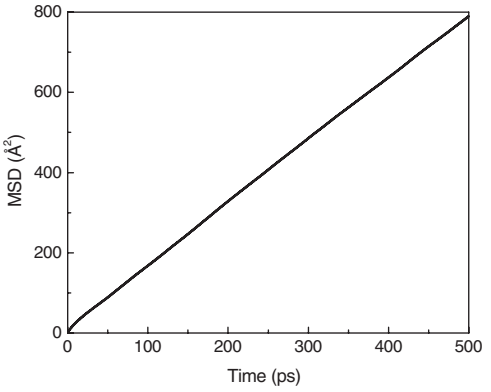

FIG. 4. Variation of mean-squared displacement (MSD) with time as obtained from the simulation.

Their integration can be related to macroscopic transport coefficients while their Fourier transforms can be related to the experimentally measured data. One such correlation function, which gives information about the translational motion of the molecules, is the velocity autocorrelation function (VACF) for the center of mass of the molecules. Figure 3 shows the velocity autocorrelation function calculated for the center of mass of 1,3-butadiene molecules in Na-Y zeolite cages. The VACF is found to have a negative region, which is indicative of the rebounding motion of molecules due to collision with the neighbors. The correlation function dies down to zero practically within a time of a few picoseconds, which is a good indication of the ergodicity of the system [23]. As noted earlier, the diffusion coefficient can be obtained from the VACF by integrating the function up to infinite time,

$$D = \frac{1}{3}\int_0^\infty \langle \boldsymbol{v}_i(t) \cdot \boldsymbol{v}_i(0)\rangle dt. \tag{2}$$

Here $\boldsymbol{v_i}(t)$ and $\boldsymbol{v_i}(0)$ are the center-of-mass velocities of the ith 1,3-butadiene molecule at times t and $t=0$, respectively, and the angular brackets denote ensemble average. In practice the upper limit of integration can be a few picoseconds by which time the correlations have all died out. The diffusion coefficient for 1,3-butadiene molecules inside Na-Y zeolite cages has been obtained by integrating the velocity autocorrelation function yielding a value of $(2.67 \pm 0.02) \times 10^{-5}$ cm^2/s for the diffusion coefficient.

In an MD simulation, the autocorrelation functions are known to have large statistical errors especially at longer times because of the limited sample size. Another mathematically equivalent way to obtain the diffusion coefficient is from the slope of the mean-squared displacement with respect to time at sufficiently long time using the Einstein relation

$$2tD = \frac{1}{3}\langle |\boldsymbol{r}_i^{\mathrm{c.m.}}(t) - \boldsymbol{r}_i^{\mathrm{c.m.}}(0)|^2\rangle, \tag{3}$$

where $\boldsymbol{r}_i^{\mathrm{c.m.}}(t)$ and $\boldsymbol{r}_i^{\mathrm{c.m.}}(0)$ are the position vectors of center of mass of the ith molecule at times t and $t=0$, respectively, and the angular brackets denote ensemble average [21]. The quantity in the angular brackets is the mean-squared displacement. The diffusion coefficient calculated from a plot of mean-squared displacements vs time (Fig. 4) for 1,3-butadiene in Na-Y zeolite is $(2.5 \pm 0.2) \times 10^{-5}$ cm^2/s which is significantly close to the value obtained from VACF implying that the small size effects are negligible.

The diffusion coefficients of propane and acetylene reported earlier from simulation are $(1.3 \pm 0.1) \times 10^{-5}$ cm^2/s and $(9.4 \pm 0.3) \times 10^{-5}$ cm^2/s, respectively. Compared to these the value of diffusion coefficient calculated above comes as an intermediate value. The QENS experiments also showed that the diffusion coefficient of 1,3-butadiene is marginally larger than that of propane in Na-Y zeolite [9]. As discussed in Ref. [9] it may be explained on the basis of planar nature of the butadiene molecule, which makes it more mobile as compared to propane, which is a smaller molecule.

Another correlation function which reveals information about the molecular motion is the intermediate scattering function $I(Q,t)$ [24]. The temporal Fourier transform of this function is the scattering law, which is proportional to the measured intensity in a neutron scattering experiment. The intermediate scattering function is thus related to the observed spectra in a neutron scattering experiment. The spatial Fourier transform of the intermediate scattering function is the van Hove correlation function $G(\boldsymbol{r}, t)$ which gives the probability of finding a particle at $\boldsymbol{r}$ at a time t given that a reference particle was present at $\boldsymbol{r}=0$ at time $t=0$. Moreover, this correlation function can then be divided into two parts. When one is interested in studying the motion of an individual particle, then one essentially talks about the probability of finding a particle at $\boldsymbol{r}$ at a time t given that the same particle was present at $\boldsymbol{r}=0$ at time $t=0$. This is the self-part of the correlation function in contrast to the distinct part where the reference particle and the particle under consideration need not be same. This division of the correlation function gives rise to a division of the scattering law into coherent and incoherent parts. In case of quasielastic neutron scattering (QENS) by hydrogenous samples it is the incoherent part that dominates because of a large incoherent scattering cross section of hydrogen. In an incoherent QENS experiment thus, the observed intensity is due to the dynamics

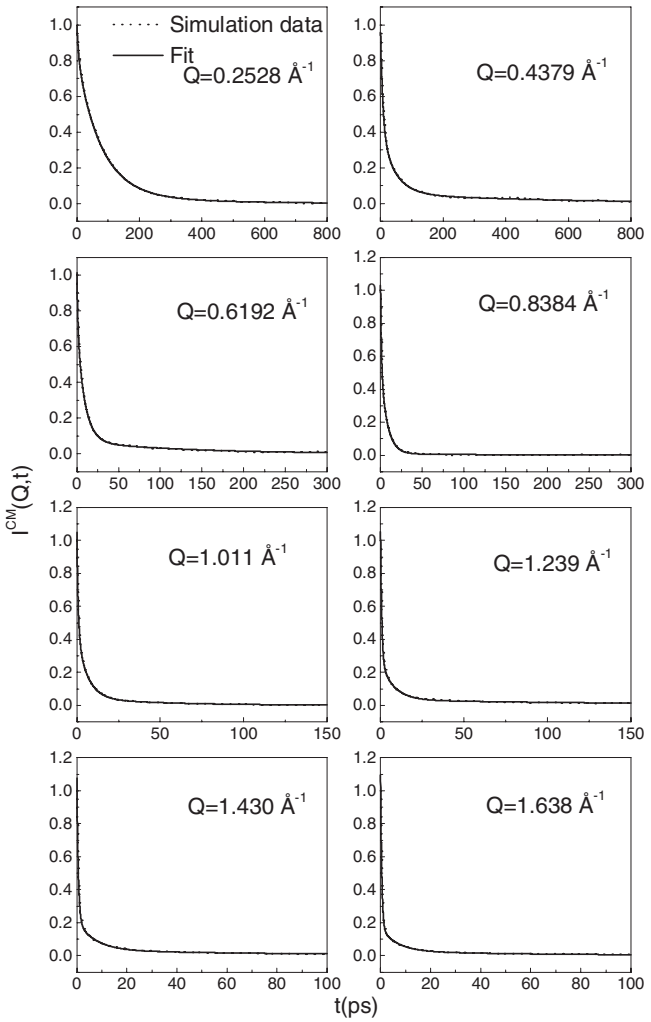

FIG. 5. The plot of the intermediate scattering function corresponding to the motion of the center of mass of the molecule $[I^{\text{c.m.}}(Q,t)]$ with time. The solid lines are the fit as obtained using the model function given in Eq. (7).

of a single particle as against the collective motion of molecules. This relation of the $I(Q,t)$ function with the observed spectra in a quasielastic neutron scattering experiment has resulted in a large number of comparisons made between QENS and MD simulation studies [25].

The intermediate scattering function can be calculated from the trajectories of a particle obtained in an MD simulation as

$$I(Q,t) = \langle \exp\{i\boldsymbol{Q} \cdot [\boldsymbol{r}_i(t+t_0) - \boldsymbol{r}_i(t_0)]\}\rangle, \tag{4}$$

where $\boldsymbol{r}_i(t+t_0)$ and $\boldsymbol{r}_i(t_0)$ denote the position vectors of the ith particle at times $t+t_0$ and t_0, respectively.

The position vector of the ith site of the 1,3-butadiene molecule in a space fixed coordinate system, $\boldsymbol{r}_i$ can be written as a sum of the position vector of the center of mass of the molecule with respect to a space fixed reference frame, $\boldsymbol{r}_i^{\text{c.m.}}$ and the position vector of the site with respect to the center of mass of the molecule $\boldsymbol{d}_i$,

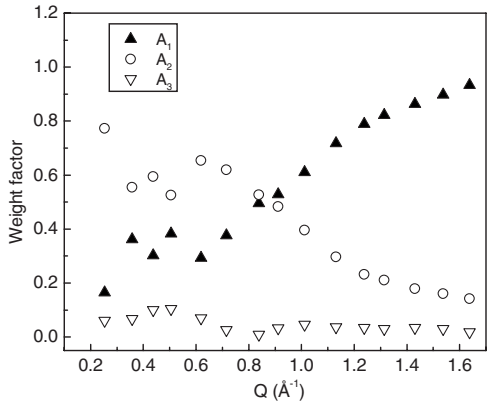

FIG. 6. Variation of weight factors $[A(Q)$'s$]$ in Eq. (7), with Q. Errors in the weight factors are smaller than the symbols used to represent them.

$$\boldsymbol{r}_i = \boldsymbol{r}_i^{\text{c.m.}} + \boldsymbol{d}_i. \tag{5}$$

To obtain information about the geometry of translational motion, the intermediate scattering function for center of mass $I^{\text{c.m.}}(Q,t)$ was calculated as

$$I^{\text{c.m.}}(Q,t) = \langle \exp\{i\boldsymbol{Q} \cdot [\boldsymbol{r}_i^{\text{c.m.}}(t+t_0) - \boldsymbol{r}_i^{\text{c.m.}}(t_0)]\}\rangle. \tag{6}$$

It may be noted that to compare with the experimental data from powder samples, one must take average over all directions [24]. Usually the decay of the intermediate scattering function is describable by an exponential function of time. A single exponential function could not describe the behavior of the intermediate scattering function, which was the case in earlier studies also [6,12]. A linear combination of exponentials and Gaussian functions was considered. We have found that in the present case of 1,3-butadiene molecules in Na-Y zeolite cages, a combination of three exponentials gives a good fit to the intermediate scattering functions over the entire range of Q and t. The model we have used is given as

$$I^{\text{c.m.}}(Q,t) = A_1(Q)e^{[-t\Gamma_1(Q)]} + A_2(Q)e^{[-t\Gamma_2(Q)]} + A_3(Q)e^{[-t\Gamma_3(Q)]}. \tag{7}$$

It is important to note here that QENS experiments on a given spectrometer measure the dynamics corresponding to the resolution of the spectrometer. The QENS spectrometer at Dhruva has an energy resolution of 200 μeV, which effectively measures time correlations of the order of 10 ps. It turns out that this dynamics corresponds to only one or more of the various components in Eq. (7). Other components may be observable at another instrument with appropriate resolution.

Figure 5 shows the fit of the $I^{\text{c.m.}}(Q,t)$ functions obtained from the simulation using Eq. (6) with the model given above in Eq. (7). The behavior of the weight factors, $A(Q)$'s, with Q is shown in Fig. 6. At lower Q values the second exponential component (II) is dominating whereas at higher Q it is the first component (I) that dominates. The third component (III) is more or less insignificant over the entire Q range. The behavior of the widths of the three exponential functions with Q is shown in Fig. 7. Also shown in the figure is the data obtained from the QENS experiment reported

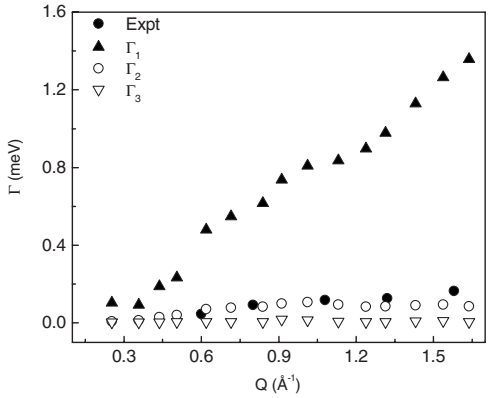

FIG. 7. Variations of the widths (Γ_1, Γ_2, and Γ_3) corresponding to the three regimes of the translational motion with Q. Error bars are smaller than the symbols.

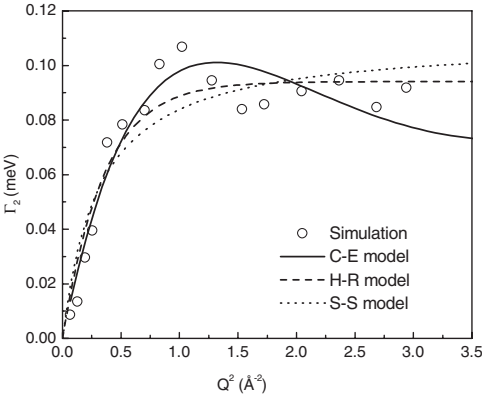

FIG. 8. Variation of Γ_2 (which correspond to the QENS results) with Q^2. Solid lines are the fit with different models described in the text. Error bars on the simulation data are smaller than the symbols.

earlier [9]. It can be seen that two exponentials (Γ_1 and Γ_3) are either too slow or too fast as compared to the time window of the QENS experimental data [9]. The weight factor corresponding to the faster component (A_1) dominates at larger Q values (Fig. 6) or equivalently at shorter length scales. A similar fast component was observed in the case of propane in Na-Y zeolite and it was attributed to the short-range rapid rattling motion at an adsorption site [6]. The second component (A_2), which has a significant contribution at short Q values or longer length scales, is the one that is responsible for the diffusive motion as observed in the QENS experiment. In case of acetylene it was the slowest component that was observed in the QENS measurement whereas in the case of propane the intermediate component of translational motion correspond to the experimental data. Since 1,3-butadiene is more akin to propane rather than acetylene, it is expected that the behavior of the component that is observed in the QENS experiments would be similar in propane and 1,3-butadiene. Indeed it is the intermediate component in the case of 1,3-butadiene just as that in propane, which is observed in the present QENS instrument at Dhruva. The weight factor associated with the third component is almost insignificant. This component represents very slow motion of molecules akin to the ones observed by Jobic *et al.* in case of xylene adsorbed in *X*-type zeolites from their NSE experiment ($D \sim 10^{-8}-10^{-9}$ cm^2/s) [17].

To investigate the geometry of the diffusion process, the widths of the intermediate component (II) that corresponds to the experimental data were fitted with three different jump diffusion models referred to in Ref. [9], as shown in Fig. 8. As can be seen from the figure the Chudley-Elliott (CE) model, which describes jump diffusion with a constant jump length explains the data better than the other two. The other two models considered here are the Hall-Ross (HR) model which corresponds to Gaussian distribution of jump length and Singwi-Sjölander (SS) model which represents random distribution of jump lengths. As shown in the potential energy landscapes earlier, the distribution of energy minima is very well ordered, the nearest-neighbor distance for the minima being constant. This gives rise to a constant jump length for the molecules jumping from one minimum to the next. The diffusion coefficients, the residence times and the jump lengths obtained from the foresaid fitting are shown in Table II. Also shown in Table II are the parameters obtained from experimental data. The fact that the jump lengths obtained from the experiments as well as from the simulation are much smaller than the cage size in all the models considered implies that the diffusion process is mainly intracage. This fact can be readily seen in Fig. 9 where the trajectories of the center of mass of a single molecule have been plotted. It can be seen that the trajectory is made up of intermittent localized regions akin to the cage structure. Within a localized region of size about 9 Å the molecule can be seen to have undergone a vigorous shuttling.

The diffusion coefficient corresponding to the component-II as obtained from the fit (CE model) is 3.2×10^{-5} cm^2/s, which is close to the overall diffusion coefficient value of 2.55×10^{-5} cm^2/s obtained from the mean-squared displacements. This indicates that the overall transport of the molecules in the zeolite is largely described by the above component-II and the CE model.

TABLE II. Comparison of the diffusion parameters obtained for 1,3-butadiene in Na-Y zeolite cages. The values of parameters obtained from a fit of all three jump diffusion models, Hall-Ross (HR), Chudley-Elliott (CE), and Singwi-Sjölander (SS), are listed for both the present simulation work and an earlier reported experiment [9]. The simulation results correspond to only the component-II in Eq. (7), which is close to that observed in the QENS experiment.

	$\langle l^2 \rangle^{1/2}$(Å)			τ(ps)			$D(10^{-5}$ cm^2/s)		
	HR	CE	SS	HR	CE	SS	HR	CE	SS
Simulation	4.1	3.9	4.4	7.0	7.9	6.0	4.1 ± 0.5	3.2 ± 0.3	5.4 ± 1.0
Experiment	2.3	2.5	2.2	3.7	4.8	2.7	2.4 ± 0.3	2.2 ± 0.2	3.0 ± 0.4

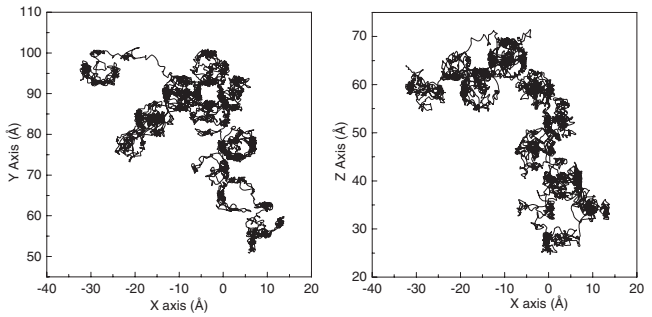

FIG. 9. Trajectory of the center of mass of one 1,3-butadiene molecule from $t=0$ to $t=1.3$ ns as obtained from the simulation. The molecule can be seen to spend a considerable amount of time confined within the cages. Within the cages, which show up as spherical regions traced by the trajectory, several sites of localization, where the trajectory looks crowded, can be seen.

In a molecular system both translational as well as rotational motions can be present. The two motions are decoupled if the intermediate scattering function corresponding to the net motion of all the atoms in a molecule can be expressed as a product of the intermediate scattering functions corresponding to the center of mass or translational and rotational motion, respectively [26], i.e.,

$$I(Q,t) = I^{\text{c.m.}}(Q,t)I^{\text{rot}}(Q,t). \tag{8}$$

The intermediate scattering function for the net motion is calculated with Eq. (4) above whereas the center-of-mass intermediate scattering function is calculated as in Eq. (6). The intermediate scattering function for rotational motion is calculated as

$$I^{\text{rot}}(Q,t) = \langle \exp\{i\boldsymbol{Q}\cdot[\boldsymbol{d}_i(t+t_0) - \boldsymbol{d}_i(t_0)]\}\rangle. \tag{9}$$

Figure 10 shows the behavior of the various intermediate scattering functions described above for $Q=1.01$ Å^{-1}. Also shown in the figure, the product of the intermediate functions corresponding to the center of mass and rotational motion, $I^P(Q,t)$, is matching very well with the net intermediate scattering function $I(Q,t)$. This shows that the assumption that

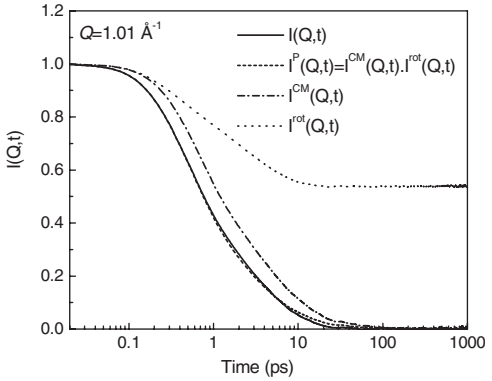

FIG. 10. Comparison of the intermediate scattering functions corresponding to the center-of-mass motion, rotational motion, net molecular motion, and the product of the former two. Very good agreement between the last two validates the assumption of decoupling of translational and rotational motions.

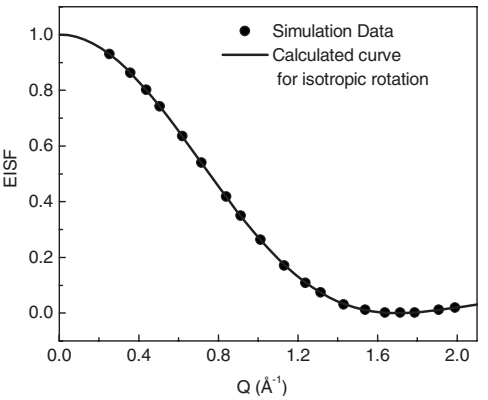

FIG. 11. Variation of EISF as obtained from the intermediate scattering function, $I^{\text{rot}}(Q,t)$, corresponding to the rotational motion of the 1,3-butadiene molecule, with Q. The solid line corresponds to that calculated for isotropic rotational motion. Errors in the simulation data are smaller than the symbols.

the translational or the center-of-mass motion and the rotational motion are decoupled is valid.

Intermediate scattering functions corresponding to rotational motion have been calculated using Eq. (9). However, since the molecule is assumed to be rigid, the information about the rotational motion obtained by following the motion of a single site would be the same as that obtained by averaging over all the atoms constituting the molecules. We have therefore followed the motion of one CH site which is at a distance of $d=1.84$ Å from the center of mass. The $I^{\text{rot}}(Q,t)$ functions were calculated for this CH site only using Eq. (9). The geometry of the rotational motion can be revealed by the

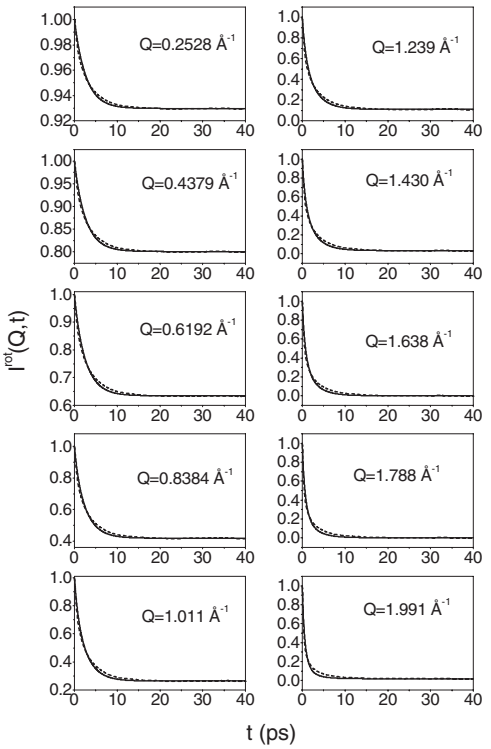

FIG. 12. Typical intermediate scattering functions, $I^{\text{rot}}(Q,t)$, fitted with isotropic rotational diffusion model at different Q values.

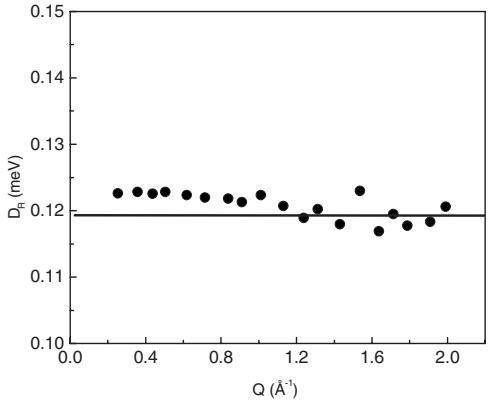

FIG. 13. Rotational diffusion coefficient as obtained from a fit of the intermediate scattering functions with the isotropic rotational diffusion model.

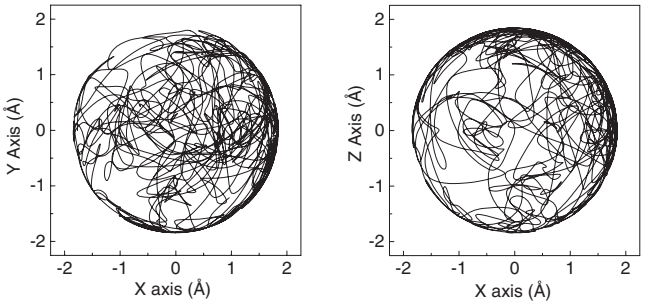

FIG. 14. Trajectory of a CH site with respect to the center of mass of the molecule for the first 100 ps of the simulation production run. The trajectory is evidently a sphere in three dimensions confirming that the rotational motion indeed is isotropic.

long-time behavior of these functions. The fact that these functions decay to nonzero values at long times indicate the fact that rotation is a localized motion. This nonzero value of the rotational intermediate scattering functions at long times is identical to the elastic incoherent structure factor (EISF) used in the analysis of QENS experimental data [24]. The behavior of EISF can be studied to gain information about the nature of rotational motion. The variation of EISF can be compared with the different models of rotational motion [24]. In case of 1,3-butadiene adsorbed in Na-Y zeolite cages, the variation of EISF is found to match very well with that corresponding to the isotropic rotational diffusion model (Fig. 11).

In isotropic rotational diffusion model the rotational motion of the molecule is assumed to occur through random discrete jumps in all possible directions. As a result, after a certain interval of time no preferred orientation of the molecule exists. The EISF in case of isotropic rotational diffusion can be expressed as $j_0^2(QR)$ where j_0 is the zeroth-order Bessel function, and R is the radius of gyration [27]. The intermediate scattering function in case of isotropic rotational diffusion can be written as

$$I^{\mathrm{rot}}(Q,t) = \sum_{l=0}^{\infty} (2l+1) j_l^2(QR) \exp[-l(l+1)D_R t], \quad (10)$$

j_l's are Bessel functions, and D_R is the rotational diffusion coefficient. The factor $(2l+1)j_l^2(QR)$ in the present case has a significant contribution only up to $l=6$ for the largest Q value of 1.99 Å^{-1} and so the summation over infinite terms in Eq. (10) can be truncated at $l=6$. The parameters (R and D_R) were obtained by least-squares fitting (Fig. 12) of the model $I^{\mathrm{rot}}(Q,t)$ [Eq. (10)] with that obtained from simulation. From the fit average values of $D_R=0.12$ meV and radius of gyration $R=1.84$ Å are obtained. The variation of D_R is shown in Fig. 13. The result that D_R does not change with Q indicates that the isotropic rotational diffusion model is a good representation for the system. This value of diffusion coefficient is smaller than that obtained earlier for propane. This is to be expected because of the smaller moment of inertia of propane molecules as compared to 1,3-butadiene molecules.

In order to examine whether the rotational motion is truly isotropic, we traced the trajectory of one of the CH sites of the molecule with respect to the center of mass. The trajectories in the X-Y and X-Z planes are shown in Fig. 14. It is clearly seen from the two figures that the path traced by the CH site with respect to the center of mass of the molecule forms the surface of a sphere thereby showing that the molecule has had all of the possible orientations during the time interval of the simulation. In other words, the rotational motion is isotropic. Moreover, since the rotational motion of propane as also that of acetylene inside Na-Y zeolite has also been reported to be isotropic it seems that the large pore size of the host plays an important role in determining the nature of rotational diffusion.

IV. CONCLUSION

Molecular dynamics simulation of 1,3-butadiene in Na-Y zeolite has been done. The simulation results show that the translational diffusion in butadiene adsorbed in Na-Y zeolite is faster as compared to propane but slower than that in the case of acetylene. The translational motion is found to be composed of three different time regimes. One of these is observable in the QENS spectrometer installed at Dhruva reactor in Trombay. The nature of the motion in this regime is found to match with the experimental results obtained earlier. The motion in this regime of translational motion is found to occur through discrete jumps with a constant jump length. Moreover, the diffusion process is found to be mainly intracage. Rotational motion is found to be isotropic as observed earlier in the case of propane and acetylene. The diffusion coefficient obtained for rotational motion is found to be smaller than that in propane, which is to be expected because of larger mass and size of 1,3-butadiene molecule.

[1] G. Tomlinson, *Modern Zeolites, Structure and Function in Detergents and Petrochemicals* (Traw Tech Publications Ltd., Switzerland, 1998).
[2] *Studies in Surface Science and Catalysis 58: Introduction to Zeolite Science and Practice*, edited by H. van Bekkum, E. M. Flanigen, and J. C. Jansen (Elsevier, New York, 1991).
[3] A. K. Tripathi, A. Sahasrabudhe, S. Mitra, R. Mukhopadhyay, and N. M. Gupta, Phys. Chem. Chem. Phys. **3**, 4449 (2001).
[4] S. Mitra, R. Mukhopadhyay, A. K. Tripathi, and N. M. Gupta, Appl. Phys. A: Mater. Sci. Process. **74**, S1308 (2002).
[5] A. Sahasrabudhe, S. Mitra, A. K. Tripathi, R. Mukhopadhyay, and N. M. Gupta, Phys. Chem. Chem. Phys. **5**, 3066 (2003).
[6] A. Sayeed, S. Mitra, A. V. Anil Kumar, R. Mukhopadhyay, S. Yashonath, and S. L. Chaplot, J. Phys. Chem. B **107**, 527 (2003).
[7] R. Mukhopadhyay, A. Sayeed, S. Mitra, A. V. Anil Kumar, M. N. Rao, S. Yashonath, and S. L. Chaplot, Phys. Rev. E **66**, 061201 (2002).
[8] S. Mitra, S. Sumitra, A. M. Umarji, R. Mukhopadhyay, S. Yashonath, and S. L. Chaplot, Pramana, J. Phys. **63**, 449 (2004).
[9] S. Gautam, S. Mitra, A. Sayeed, S. Yashonath, S. L. Chaplot, and R. Mukhopadhyay, Chem. Phys. Lett. **442**, 311 (2007).
[10] S. Mitra, Siddharth Gautam, R. Mukhopadhyay, S. Sumitra, A. M. Umarji, S. Yashonath, and S. L. Chaplot, Physica B (Amsterdam) **385–386**, 275 (2006).
[11] Pradip Kr. Ghorai, Subramanian Yashonath, Pierfranco Demontis, and Giuseppe B. Suffritti, J. Am. Chem. Soc. **125**, 7116 (2003).
[12] Siddharth Gautam, S. Mitra, R. Mukhopadhyay, and S. L. Chaplot, Phys. Rev. E **74**, 041202 (2006).
[13] D. Dubbeldam and R. Q. Snurr, Mol. Simul. **33**, 305 (2007).
[14] P. Demontis and G. B. Suffritti, Chem. Rev. **97**, 2845 (1997).
[15] D. Keffer, Alon V. McCormick, and H. Ted Davis, J. Phys. Chem. **100**, 967 (1996).
[16] J. Kärger and D. M. Ruthven, *Diffusion in Zeolites and Other Microporous Solids* (Wiley-Interscience, New York, 1992).
[17] H. Jobic, Alain Méthivier, and Georg Ehlers, Microporous Mesoporous Mater. **56**, 27 (2002).
[18] H. Jobic, Harikrishnan Ramanan, Scott M. Auerbach, Michael Tsapatsis, and Peter Fouquet, Microporous Mesoporous Mater. **90**, 307 (2006).
[19] A. N. Fitch, H. Jobic, and A. Renouprez, J. Phys. Chem. **90**, 1311 (1986).
[20] S. Calero, D. Dubbeldam, R. Krishna, B. Smit, T. J. H. Vlugt, J. F. M. Denayer, J. A. Martens, and T. L. M. Maesen, J. Am. Chem. Soc. **126**, 11377 (2004).
[21] M. P. Allen and D. J. Tildesley, *Computer Simulation Of Liquids* (Oxford University Press, Oxford, 1987).
[22] W. L. Jorgensen, J. D. Madura, and C. J. Swenson, J. Am. Chem. Soc. **106**, 6638 (1984).
[23] M. Evans, Gareth Evans, William T. Coffey, and Paolo Grigolini, *Molecular Dynamics and Theory of Broad Band Spectroscopy* (Wiley-Interscience, New York, 1982).
[24] M. Bée, *Quasi-Elastic Neutron Scattering* (Adam Hilger, Bristol, 1988).
[25] H. Jobic and D. N. Theodorou, Microporous Mesoporous Mater. **102**, 21 (2007).
[26] D. Di Cola, A. Deriu, M. Sampoli, and A. Torcini, J. Chem. Phys. **104**, 4223 (1996).
[27] V. F. Sears, Can. J. Phys. **44**, 1999 (1996).